Magnetic properties of metastable Zr-Ni and Hf-Ni alloys around the paramagnetic-ferromagnetic transition

I. Bakonyi,* L. F. Kiss, E. Varga,† and L. K. Varga
Research Institute for Solid State Physics and Optics, Hungarian Academy of Sciences, H-1525 Budapest, P.O.B. 49, Hungary
(Received 17 April 2004; revised manuscript received 30 August 2004; published 4 January 2005)

A melt-spinning technique was used to produce metastable Zr-Ni and Hf-Ni alloys for compositions around the Ni-rich eutectic (at 89, 90, and 91 at. % Ni content). Depending on the cooling rate and alloy composition, either an amorphous (a) or a body-centered-cubic (bcc) phase or a nanocrystalline (*n*) state with the $(Zr,Hf)Ni_5$ structure was formed. In this paper, experimental results on the low-temperature magnetic properties of these Zr-Ni and Hf-Ni ribbons are presented. The ac susceptibility, the low-field magnetization, and the magnetization isotherms were measured between 5 and 300 K. The Curie points of the amorphous and bcc phase of the Zr_9Ni_{91} alloy were practically the same (about 70 K) and the T_C of the *a*-$Zr_{10}Ni_{90}$ alloy was around 42 K, whereas the *n*-$Hf_{11}Ni_{89}$ alloy remained Pauli paramagnetic down to 5 K. The results are evaluated in the framwork of the theory of very weak itinerant ferromagnetism. The critical concentration of Ni for the onset of ferromagnetism in these metastable alloys was deduced to be about 89.5 at. % Ni. The characteristics of the paramagnetic-ferromagnetic transition in these systems are discussed in terms of the electronic density of states at the Fermi level.

DOI: 10.1103/PhysRevB.71.014402 PACS number(s): 75.50.Kj, 71.23.Cq

I. INTRODUCTION

The magnetic properties of alloys of Ni with several early transition metals such as Mo,[1] V,[1,2] or Y (Refs. 3 and 4) have been extensively investigated, especially as far as their behavior around the critical concentration of the paramagnetic-ferromagnetic (PM-FM) transition is concerned. This transition typically occurs for Ni concentrations in the range 80–90 at. %. In the Zr-Ni and Zr-Hf systems, however, studies reporting on the magnetic properties in the composition range where the PM-FM transition can be expected to occur have remained rather scarce to date and even these results are contradictory to some extent.

Amamou *et al.*[5] reported that the most Ni-rich compound in the Zr-Ni system, $ZrNi_5$, remains Pauli paramagnetic down to at least 4.2 K. In line with this finding, Turek *et al.*[6] found the absence of ferromagnetism for the crystalline $ZrNi_5$ phase by using electronic band-structure calculations and the same result was obtained for the amorphous (*a*) $Zr_{15}Ni_{85}$ alloy as well. Pauli paramagnetism was deduced also for a nanocrystalline (*n*) $Hf_{11}Ni_{89}$ alloy with the $HfNi_5$ structure.[7]

On the other hand, ferromagnetism was observed for melt-quenched *a*-$Zr_{10}Ni_{90}$ (Ref. 8) and *a*-Zr_9Ni_{91} (Ref. 9) alloys and for sputtered amorphous Zr-Ni alloys[10] for Ni contents from 88 to 92 at. %. However, the Curie temperatures (T_C) for the two melt-quenched alloys differed strongly both from each other and from the values of the corresponding sputtered samples. Furthermore, it was established[9] that in a melt-quenched Zr_9Ni_{91} alloy, which was produced as a solid solution of Zr in Ni with a body-centered-cubic (bcc) structure, the Curie point was practically the same as the value for the *a*-Zr_9Ni_{91} ribbon.

The discrepancies between the results on the different metastable Ni-rich Zr-Ni alloys have motivated the present detailed magnetization study. It was also of interest to compare the magnetization characteristics of the amorphous and bcc phases with the same chemical composition in more detail and to extend the study of magnetic properties to other available Zr-Ni and Hf-Ni alloy compositions. Another aim was to establish the critical concentration for the PM-FM transition in these alloy systems.

In this paper, experimental results on the temperature dependence (from 5 to 300 K) of the ac susceptibility, the low-field magnetization, and the magnetization isotherms up to 50 kOe are presented for structurally well-characterized melt-quenched Zr-Ni and Hf-Ni ribbons. By detailed analysis of the results obtained, the magnetic transition temperatures and the matrix saturation magnetization values, the temperature evolution of the coercive fields, and high-field susceptibility could be deduced. The behavior of the FM alloys was interpreted in terms of very weak itinerant ferromagnetism (VWIF).[11] From the composition dependence of the Curie point, the critical concentration of the PM-FM transition was found to be around 89.5 at. % Ni for (Zr,Hf)-Ni alloys. Some information concerning the influence of metallurgical heterogeneities on the observed magnetic transition temperatures could also be derived from these studies. It is believed that the present work provides an as complete as possible picture about the current understanding of the magnetic properties in the various structural modifications of Ni-rich alloys in the Zr-Ni and Hf-Ni systems.

The paper is organized as follows. Section II describes the details of sample preparation and magnetic measurements. The magnetization data and their analysis are presented in Sec. III. These results are discussed in Sec. IV in terms of the electronic density of states (DOS) for Ni-rich Zr-Ni and Hf-Ni alloys as well as the characteristics of the PM-FM transition in these systems. Finally, the conclusions are summarized in Sec. V.

II. EXPERIMENT

The metastable Zr-Ni and Hf-Ni alloy ribbons were produced by a melt-spinning technique. The ribbon preparation details[12] and the structural characterization[7,12–16] have been described elsewhere. Depending on their thickness (i.e., on the cooling rate), ribbons with an amorphous structure (a-$Zr_{10}Ni_{90}$ and a-Zr_9Ni_{91}), a bcc Ni(Zr) solid solution phase (bcc-Zr_9Ni_{91}) or a nanocrystalline state (n-$Hf_{11}Ni_{89}$) were obtained. The ribbons will be identified by the same code numbers as introduced in Ref. 12.

The magnetization (σ) isotherms were measured in magnetic fields up to 16 kOe below room temperature in a vibrating sample magnetometer (VSM). The same apparatus was used to measure the low-field (10 Oe) magnetization as a function of increasing temperature after either zero-field cooling (ZFC) or field-cooling (FC) in a magnetic field of 10 Oe. For an amorphous (a-Zr_9Ni_{91}) and a nanocrystalline (n-$Hf_{11}Ni_{89}$) ribbon, the magnetization isotherms were measured in a superconducting quantum interference device magnetometer up to 50 kOe and the temperature dependence of the coercive force was studied for the amorphous alloy. The real component of the ac susceptibility (χ_{ac}) was studied at 6 kHz frequency with $H_{max}=20$ mOe from 5 to 300 K. These latter measurements were performed in a home-built ac susceptometer in which the probe was manually lifted up or down above the liquid-He level in a cryostat in order to increase or decrease the sample temperature, respectively. The ac-susceptibility runs were mostly recorded with decreasing temperature.

III. RESULTS AND DATA ANALYSIS: FIELD AND TEMPERATURE DEPENDENCE OF MAGNETIZATION

A. Low-field magnetization and ac susceptibility data

The results of low-field magnetization (σ) and ac-susceptibility (χ_{ac}) measurements for the a-$Zr_{10}Ni_{90}$ and a-Zr_9Ni_{91} alloys are summarized in Fig. 1. The sharp changes of both σ and χ_{ac} around 40 and 70 K, respectively, indicate well-defined PM-FM transitions for both alloys. The small difference between the FC and ZFC low-field magnetization data suggests that the matrix of these alloys has a good magnetic homogeneity and it exhibits a clear FM behavior. The shape of the χ_{ac} curves is also characteristic of the appearance of a normal FM phase below the transformation temperatures.

The Curie point can be estimated by linearly extrapolating the $\sigma(T)$ and $\chi_{ac}(T)$ curves to the temperature axis as indicated by the solid line for the χ_{ac} data of the a-$Zr_{10}Ni_{90}$ alloy in Fig. 1. The analysis of the low-field magnetization/ac-susceptibility data yields $T_C=41$ K/42 K for a-$Zr_{10}Ni_{90}$ and $T_C=66$ K/69 K for a-Zr_9Ni_{91}. The difference in the T_C values from the a-$Zr_{10}Ni_{90}$ to the a-Zr_9Ni_{91} alloys is ascribed to the higher Ni content of the latter one. The present results are in good agreement with our previous χ_{ac} measurements[9] on another piece of the same a-Zr_9Ni_{91} ribbon (no. 267) where $T_C=66$ K was obtained.

The low-field magnetization and χ_{ac} data for the bcc-Zr_9Ni_{91} alloy are shown in Fig. 2(a). The ac susceptibility

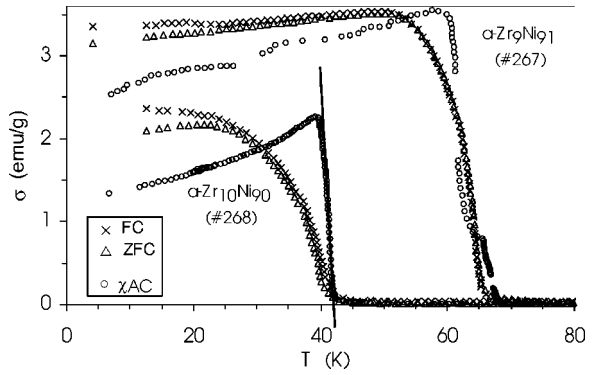

FIG. 1. Temperature dependence of the FC and ZFC low-field magnetization σ and the ac susceptibility χ_{ac} of the a-$Zr_{10}Ni_{90}$ alloy (ribbon no. 268) and the a-Zr_9Ni_{91} alloy (ribbon no. 267). For the low-field magnetization, both the measuring and cooling field were 10 Oe. The ac susceptibility is displayed in arbitrary units. The stepwise changes in the χ_{ac} data just below T_C occurred due to the manual control of the temperature. The solid line along the χ_{AC} data for a-$Zr_{10}Ni_{90}$ indicates the determination of the Curie temperature.

for two independently prepared ribbons (nos. 62 and 63), melt quenched under identical conditions from the same ingot,[12] indicates a very similar magnetic behavior, with a slight difference only of the $T_C(\chi_{ac})$ values: 69 K (no. 62) and 73 K (no. 63). The break in the low-field magnetization curves of ribbon no. 62 indicates a T_C of about 66 K for both the FC and ZFC cases. A previous low-field magnetization study[9] of another piece of ribbon no. 63 yielded a T_C of 70 K for the majority phase, in good agreement with the present work.

As shown by Fig. 2(a), however, the magnetic behavior of the bcc-Zr_9Ni_{91} alloy is somewhat different from that of the a-$Zr_{10}Ni_{90}$ and a-Zr_9Ni_{91} alloys even though the T_C of the majority phase is practically the same for the amorphous and bcc structural modifications for the Zr_9Ni_{91} alloy composition. One difference is that the peak of the χ_{ac} curves is less sharp and more broadened for the bcc ribbons. Another feature is that, besides the Curie point of the bcc matrix around 70 K, there is another sizeable magnetic transition in the bcc ribbon around 150 K as indicated by Fig. 2(b). The large difference between the FC and ZFC curves for the bcc ribbon no. 62 [Fig. 2(a)] can be ascribed to this second component, which is not characteristic of a ferromagnetic phase. This is demonstrated in Fig. 2(b) where the FC curves of the bcc-Zr_9Ni_{91} ribbon (no. 62) are shown for two different cases. In one case, the magnetization was measured with increasing temperature after the sample was cooled in a magnetic field whereby the measurement was performed with a magnetic field oriented parallel to the cooling field [curve denoted by FC(+10 Oe)]. In the other case, the measurement was performed with the same magnetic-field orientation as before but now the cooling field orientation was reversed [curve denoted by FC(−10 Oe)]. The FC curves are drastically different for the two orientations of the cooling field (+10 Oe and −10 Oe). Evidently, the phase with the transition temperature around 150 K is completely frozen in for a cooling field of 10 Oe in magnitude and the magnetization contribution of the ordinarily FM phase ($T_C=66$ K) is super-

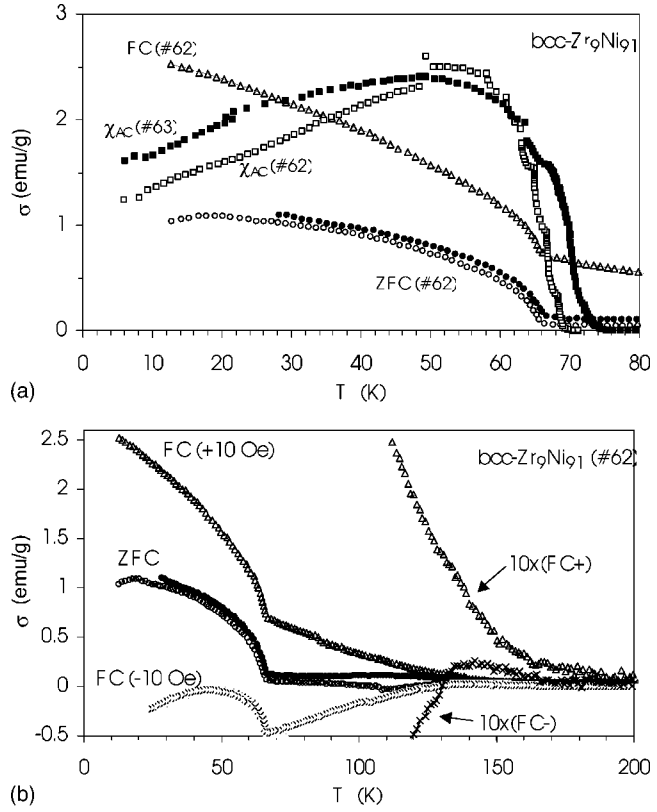

FIG. 2. (a) Temperature dependence of the FC and ZFC low-field magnetization σ and the ac susceptibility χ_{ac} of two bcc -Zr_9Ni_{91} alloys (ribbon no. 62 and ribbon no. 63). For the low-field magnetization, both the measuring and cooling field were 10 Oe (for ribbon no. 62, two ZFC measurements were performed; for details see text). The ac susceptibility is displayed in arbitrary units. The stepwise changes in the χ_{ac} data just below T_C occurred due to the manual control of the temperature; (b) Temperature dependence of the FC and ZFC low-field magnetization σ for one of the bcc-Zr_9Ni_{91} alloy samples (ribbon no. 62) shown in a larger temperature range. The two ZFC curves and the FC(+10 Oe) curve are identical to those shown in (a). For curve FC(−10 Oe), see text. Around 150 K, the FC(+10 Oe) and FC(−10 Oe) data are displayed also by magnifying them 10 times in order to better identify the magnetic transition temperature in this range.

imposed on it. The small splitting of the two ZFC curves around 100 K [Fig. 2(b)] is due to the fact that the remanence field of the VSM electromagnet was not completely zero in either case during cooling, i.e., there was a small negative nonzero magnetic field during cooling for the circle data run and a much smaller positive remanence field for the full circle data run (the measuring field was positive in both cases).

The magnetic behavior of another piece of the bcc-Zr_9Ni_{91} ribbon (no. 63) previously studied[9] was qualitatively the same: a small magnetization contribution from a phase with a transition temperature of about 130 K and a majority FM phase with $T_C \approx 70$ K.

According to structural studies,[12,13] in these bcc-Zr_9Ni_{91} ribbons the dominant phase is a bcc-Ni(Zr) solid solution with fairly large ($\geqslant 0.5$ μm) crystallites of well-defined polygonal shape. Therefore the magnetic transition with $T_C \approx 70$ K in the bcc ribbons may be ascribed to this phase. This observation indicates that the Curie points of an a-Zr_9Ni_{91} alloy and a bcc-Ni(Zr) solid solution with the same chemical composition are practically the same.

Although the broad x-ray diffraction (XRD) lines suggested[13] the possible presence of some residual amorphous phase in these bcc-Zr_9Ni_{91} ribbons, no indication of an amorphous phase was obtained in the conventional TEM studies.[12,13] Based on high-resolution TEM results, it was rather suggested[13] that the XRD line broadening may come from a nanoscale structure within the interior of the bcc grains: well-ordered nanoscale regions appeared embedded in a matrix with disordered atomic positions. The ordered and disordered regions may correspond to areas with either low or high Zr contents. It may be therefore that the magnetic transition around 150 K is connected with these compositional fluctuations within the bcc crystallites.

The χ_{ac} data did not indicate the onset of FM ordering down to 5 K for the n-$Hf_{11}Ni_{89}$ alloy with the $HfNi_5$ structure (ribbon no. 277). This agrees with the result of our previous work[7] for this alloy. This means that the matrix of the n-$Hf_{11}Ni_{89}$ alloy exhibits Pauli paramagnetism.

The χ_{ac} measurements, furthermore, revealed for the a -Zr_9Ni_{91} alloy another magnetic transition in the form of a susceptibility maximum around 270 K. This might be indicative of a very small amount of Ni-rich segregations in the matrix. These features are discussed later in Sec. III C.

B. Magnetization isotherms: Arrott plot analysis

The magnetization isotherms for the a-Zr_9Ni_{91} alloy are shown in Fig. 3. They indicate the development of a spontaneous magnetization at sufficiently low temperatures and nonlinear magnetization curves for temperatures in the vicinity of the PM-FM transition. This behavior, together with the relatively low values of the magnetization and the Curie point, is typical for VWIF materials.[11] Well above the Curie point ($T_C \approx 70$ K), the magnetization isotherms are linear with a high-field susceptibility decreasing with increasing temperature. The very small (about 0.05 emu/g) apparent saturation magnetization in the PM phase [see Fig. 3(b)] is most probably of extrinsic origin, e.g., due to oxide impurities on the sample holder and therefore in the following it will be considered as a "background" magnetization only.

For the a-$Zr_{10}Ni_{90}$ alloy, the behavior of the magnetization isotherms was very similar to those for the a-Zr_9Ni_{91} alloy [Fig. 3(a)] except that the magnetization values were smaller by about a factor of 2 due to the reduced Ni content. For the bcc-Zr_9Ni_{91} alloy, the magnetization isotherms remained nonlinear up to higher magnetic fields than for a-Zr_9Ni_{91} and become linear around room temperature only.

The magnetization isotherms were evaluated with the help of Arrott plots. The linear sections at high magnetic field of the σ^2 vs H/σ plots shown in Fig. 4 for the bcc-Zr_9Ni_{91} alloy were extrapolated to $H=0$ and the intersections with the ordinate provided the spontaneous magnetization $\sigma(0,T)$. According to the theory of VWIF,[11] by plotting $\sigma^2(0,T)$ against T^2, the Curie temperatures can be determined as shown in Fig. 5: $T_C=45$ K (a-$Zr_{10}Ni_{90}$), $T_C=72$ K (a-Zr_9Ni_{91}), and

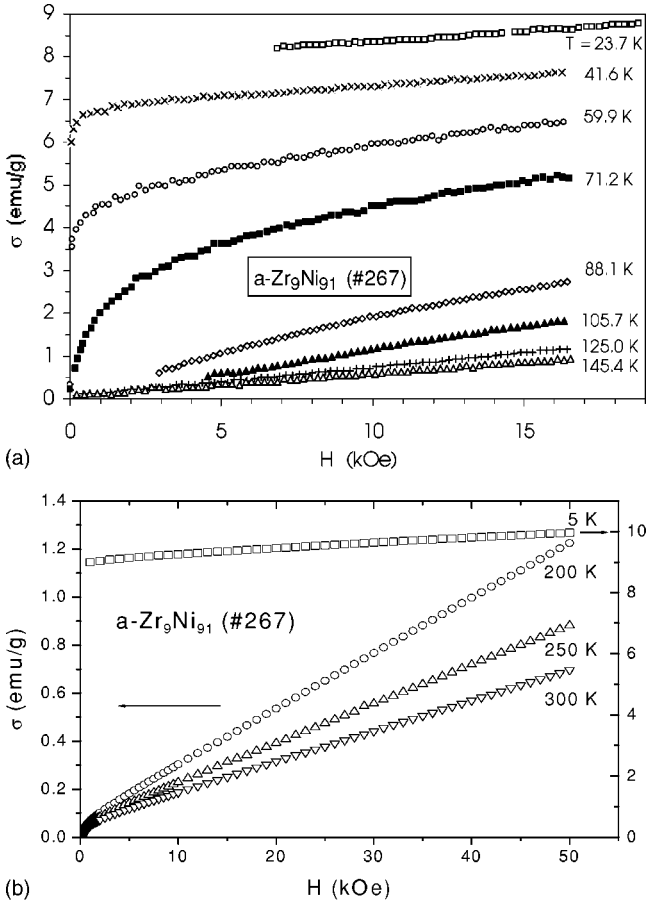

FIG. 3. Low-temperature magnetization isotherms for the a-Zr_9Ni_{91} alloy (a) for $T=23.7$ to 145.4 K up to $H=16$ kOe and (b) for $T=5$ K to 300 K up to $H=50$ kOe.

$T_C=96$ K (bcc-Zr_9Ni_{91}). For the two amorphous alloys, the T_C values are higher by about 5 K than the Curie points derived from the low-field magnetization and ac-susceptibility measurements. On the other hand, for the bcc-Zr_9Ni_{91} alloy, the Arrott plot analysis yields a much higher Curie point (the difference amounting to nearly 30 K, the relative difference corresponding to more than 40%). This latter deviation is attributed to the presence of a large amount of magnetic inhomogeneities in the bcc alloy as detected by the low-field magnetization and ac-susceptibility

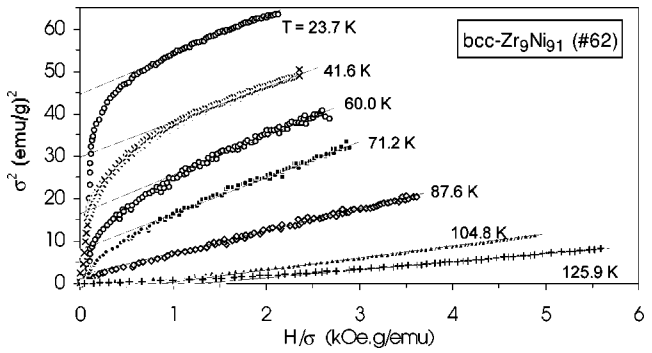

FIG. 4. Arrott plots $\sigma_2(H,T)$ vs $H/\sigma(H,T)$ of the bcc-Zr_9Ni_{91} alloy around the magnetic transition temperature.

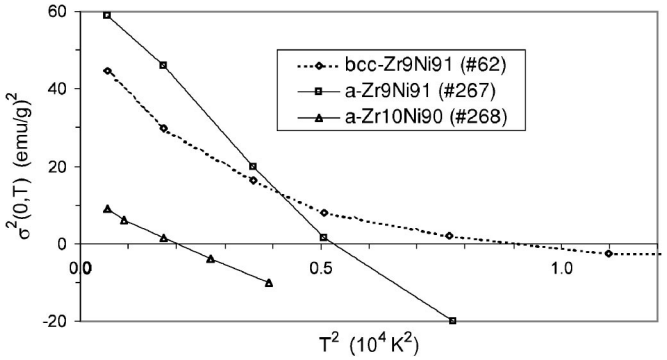

FIG. 5. Temperature dependence of the spontaneous magnetization $\sigma(0,T)$ displayed in the form of a $\sigma^2(0,T)$ vs T^2 plot for the a-$Zr_{10}Ni_{90}$, a-Zr_9Ni_{91} and bcc-Zr_9Ni_{91} alloys. The $\sigma^2(0,T)$ values are intercepts extrapolated from the Arrott plots. The lines through the data points serve as a guide for the eye only. The Curie point is identified by the temperature where $\sigma^2(0,T)$ becomes 0.

measurements (Fig. 2), in line with recent results on amorphous Ni-P (Ref. 17) and Ni(Fe)-B (Ref. 18) alloys around the PM-FM transition.[17,18] According to the analysis by Acker and Huguenin,[2] the Arrott plot evaluation can overestimate the magnetic transition temperatures for a FM matrix containing regions with a T_C higher than the matrix Curie point. This is certainly due to the fact that when approaching the T_C of the matrix with increasing temperature, the contribution of the magnetic inhomogeneities yields a $\sigma^2(0,T)$ value higher than the actual value of the FM matrix itself and this causes the curvature of the $\sigma^2(0,T)$ vs T^2 plot for such systems (see the data for bcc-Zr_9Ni_{91} in Fig. 5). In contrast, the $\sigma^2(0,T)$ vs T^2 plots are nicely linear for the a-$Zr_{10}Ni_{90}$ and a-Zr_9Ni_{91} alloys (Fig. 5).

The magnetization isotherms were measured for the n-$Hf_{11}Ni_{89}$ alloy up to $H=50$ kOe at $T=5$, 200, 250, and 300 K (Fig. 6). Although this alloy was found to exhibit Pauli paramagnetism according to the χ_{ac} data (Sec. III A), here we can see the contribution of a phase being magnetic at room-temperature and certainly even above. The room-temperature magnetization isotherm presented in Fig. 6 agrees well with

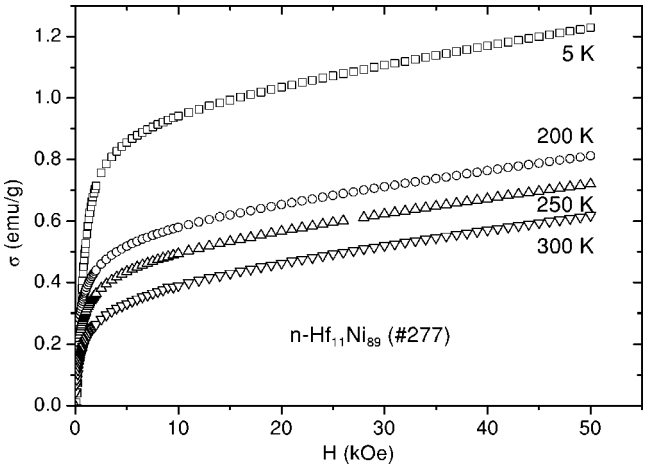

FIG. 6. Low-temperature magnetization isotherms for the n-$Hf_{11}Ni_{89}$ alloy for $T=5-300$ K up to $H=50$ kOe.

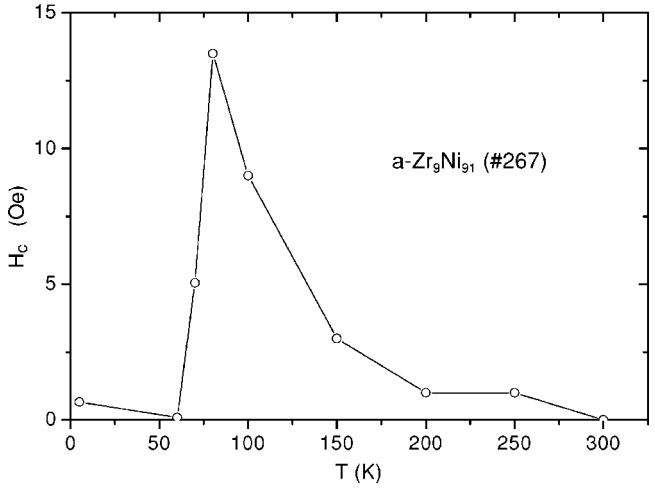

FIG. 7. Temperature dependence of the coercive force H_c for the a-Zr_9Ni_{91} alloy.

our previous data on this alloy[7] and is comparable to the magnitude of the room-temperature magnetization measured for the a-Zr_9Ni_{91} alloy [Fig. 3(b)]. This magnetic contribution can be ascribed to the presence of Ni-rich regions in the Pauli paramagnetic alloy ribbon as discussed in the next section.

C. Analysis of the magnetic inhomogeneity contributions in a-Zr_9Ni_{91} and n-$Hf_{11}Ni_{89}$

It was indicated by the previously described magnetic measurements that in these Ni-rich melt-quenched metastable Zr-Ni and Hf-Ni alloys, there are regions which are magnetic even above the T_C of the FM matrix (Zr-Ni) or they exist in the otherwise non-FM matrix (Hf-Ni).

In order to further characterize the magnetic inhomogeneities in the a-Zr_9Ni_{91} alloy (ribbon no. 267), the hysteresis loops were measured from 5 to 300 K. The hysteresis loops at 5 and 60 K, i.e., in the FM state of the amorphous matrix, were almost completely rectangular with relative remanence values very close to unity and with small coercive fields (H_c about 1 Oe or less, see Fig. 7).

Above the Curie point of the amorphous matrix ($T_C \approx 70$ K), a FM component superimposed on the small "background" magnetization (cf. Sec. III B) could still be observed, which can be ascribed to the presence of regions more rich in Ni and therefore having higher magnetic transition temperatures than the a-Zr_9Ni_{91} matrix. This FM component exhibited a sheared hysteresis loop and its H_c first increased then decreased with temperature as shown in Fig. 7. The temperature evolution of H_c for the a-Zr_9Ni_{91} alloy strongly resembles the behavior of FINEMET-type partially crystallized alloys[19] in which Fe(Si) nanoparticles are embedded in a residual amorphous matrix. Upon increasing the temperature to above the matrix T_C, the so-called "exchange softening" effect is strongly reduced and the coercive field of the remaining FM component starts to increase towards the intrinsic H_c value of the nanoparticle assembly. If the embedded particles are so small that their blocking temperature is below the matrix T_C then they exhibit superparamagnetic (SPM) characteristics for $T > T_C$ and no hysteresis occurs for such particles. However, an assembly of such particles can still exhibit FM behavior as a consequence of interparticle interactions either directly via their magnetic dipolar fields and/or indirectly via a residual exchange coupling through the paramagnetic matrix. Above about 80 K (Fig. 7), H_c starts to decrease since the interparticle coupling can diminish by a weakening of the indirect exchange interaction and also by the reduction of the direct dipolar coupling due to higher thermal agitation of the magnetization. In the temperature range 200–300 K, the very small coercive field values indicate that the coupling between the particles may have nearly completely disappeared and most of them exhibit here SPM behavior due to their small size.

The above described picture for explaining the temperature evolution of the H_c of the magnetic inhomogeneities conforms well with the χ_{ac} results for the a-Zr_9Ni_{91} ribbon (see Sec. III A). Namely, due to the extremely small (26 mOe) exciting field amplitude of the χ_{ac} measurement, the FM phase with H_c values as shown in Fig. 7 above the T_C of the amorphous matrix remains unrevealed. The magnetic inhomogeneities can be observed in the χ_{ac} measurement only if their coercive field takes very small values, i.e., for temperatures $T > 200$ K where they gradually become an assembly of independent SPM particles. This is just the temperature range where a χ_{ac} maximum occurred for this alloy.

It is noted finally that the linearity of the high-field slope of the magnetization isotherms in Fig. 3(b) indicates that this field-dependent magnetization contribution originates from the paramagnetism of the amorphous matrix and not from the SPM particles.

In the n-$Hf_{11}Ni_{89}$ alloy, the magnetization isotherms are highly nonlinear up to 50 kOe (Fig. 6). Since the alloy matrix has a $HfNi_5$ structure and shows no PM-FM transition down to 5 K, the fraction of excess Ni which is not dissolved on the Hf sites of the matrix is enriched in the intergranular phase. These regions can exhibit FM or SPM behavior, depending on their size. Therefore we have attempted to fit the magnetization curves by assuming a FM, a SPM, and a paramagnetic contribution, the latter one due to the Pauli paramagnetic matrix. Since the FM regions are expected to saturate in a few kOe magnetic field, they were taken into account by a constant magnetization contribution and the fit was made for magnetic fields above 2 kOe only. The fit results can be summarized as follows. The paramagnetic contribution was characterized by a high-field susceptibility of about $\chi_{HF} = 5 \times 10^{-6}$ emu/g for $T = 200-300$ K and 6×10^{-6} emu/g for $T = 5$ K. The average SPM magnetic moment size was about $50\mu_B$ for $T = 5$ K and about 1300, 1500, and $1600\mu_B$ for $T = 200$, 250, and 300 K, respectively. The FM saturation magnetization was 0.56 emu/g for $T = 5$ K and 0.38, 0.31, and 0.22 emu/g for $T = 200$, 250, and 300 K, respectively. These data can be interpreted by saying that the measured magnetization (Fig. 6) is dominated by the FM contribution which increases with decreasing temperature. This increase comes mainly from the fact that whereas for temperatures from 200 to 300 K part of the magnetic inhomogeneities are in the form of SPM regions with average moments around $1500\mu_B$, those large SPM regions which

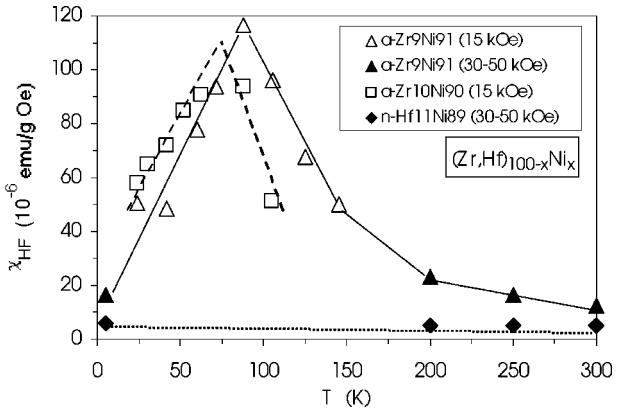

FIG. 8. Temperature dependence of the high-field susceptibility χ_{HF} for the Ni-based alloys investigated in this work.

have their blocking temperature in the range 5–200 K become ferromagnetic at the lowest temperature investigated and only the region with the smallest moments (about $50\mu_B$) remain in the SPM state at 5 K.

Recent high-precision x-ray diffraction measurements[16] indicated the presence of a small amount of a Ni [or a Ni-rich Ni(Hf) solid solution] phase in the *n*-$Hf_{11}Ni_{89}$ alloy. Since high-resolution transmission electron microscopy[15] was not able to reveal and locate a second phase beside the $HfNi_5$ structure in this alloy, it can be assumed[7] that these Ni-rich regions revealed by the magnetization data must constitute part of the intergranular phase (grain boundaries, triple-line junctions, quadrupole nodes).

D. High-field susceptibility data

From the magnetization isotherms, the high-field susceptibility χ_{HF} data can be obtained and the results are shown in Fig. 8. For the two amorphous Zr-Ni alloys, the χ_{HF} data indicate a maximum between 50 and 100 K, with the position of the maximum being higher for *a*-Zr_9Ni_{91}. This behavior is typical for ferromagnets in that a χ_{HF} maximum occurs in the vicinity of T_C, here in both cases at temperatures somewhat above T_C. On the other hand, no such maximum occurs for *n*-$Hf_{11}Ni_{89}$ since its T_C is expected to be below 5 K. The previously reported $\chi_{HF}(300\ \mathrm{K})=5.3\times10^{-6}$ emu/g value for another piece of the *n*-$Hf_{11}Ni_{89}$ ribbon[7] is in good agreement with the present data. It should also be mentioned that the value $\chi_{HF}(300\ \mathrm{K})=5\times10^{-6}$ emu/g obtained here corresponds to 360×10^{-6} emu/mol for the *n*-$Hf_{11}Ni_{89}$ alloy with the $HfNi_5$ structure whereas Amamou *et al.*[5] reported 247×10^{-6} emu/mol for the crystalline stoichiometric compound $ZrNi_5$ (composition: $Zr_{16.7}Ni_{83.3}$). As discussed below in Sec. IV A, the replacement of Zr and Hf with each other does not significantly modify the electronic structure around the Fermi level. Therefore these susceptibility data are well in accord with the 6 at. % difference in the Ni content of the two alloys.

IV. DISCUSSION

A. Features of the DOS in (Zr,Hf)-Ni alloys

In alloys of early transition metals (TE) such as Zr or Hf with late transition metals such as Ni, the electronic states associated with *d* electrons of TL metals lie at lower energies than the *d*-electron states of TE metals. This is mainly due to the differences between the energies of the corresponding atomic *d* levels. E.g., the energy of the atomic 3*d* levels of Ni is −15.23 eV and of the atomic 4*d* levels of Zr is −7.07 eV.[20] This split nature of the *d* states has, indeed, been observed by photoemission studies and confirmed by band-structure calculations. As summarized in detail in Ref. 21, it turned out from these experimental and theoretical studies that the TL *d* states form a peak below the Fermi energy E_F whereas the TE *d* states occupy mostly the region around and above E_F. As a consequence, when increasing the TL content the DOS at E_F decreases since the fraction of TE atoms contributing to this energy range decreases. The composition evolution of the DOS at E_F as deducted from low-temperature specific-heat and superconductivity data for (Ti,Zr,Hf)-(Ni,Cu) alloys up to about 70 at. % Ni or Cu has indeed been found to follow this behavior[21] and the results of reported band-structure calculations have also confirmed these findings.

The present study deals with (Zr,Hf)-Ni alloys with Ni contents around 90 at. %. In this composition range, due to the reduced TE content the Fermi level already occupies a position around the top of the Ni 3*d* band. The contribution of Zr and Hf to the DOS at E_F is small or negligible since these 4*d* and 5*d* states mostly lie above E_F. Specifically, whereas for the crystalline $ZrNi_3$ compound the Fermi level lies in a pseudogap between a large Ni 3*d* DOS peak and a small Zr 4*d* DOS peak,[22] for the $ZrNi_5$ compound the Fermi level already cuts the falling flank of the Ni 3*d* DOS peak.[6] The latter situation holds also for *a*-$Ni_{85}Zr_{15}$.[6] This is the highest Ni content for which band-structure calculation has been reported in the amorphous Zr-Ni alloy system.

An ultraviolet photoemission spectroscopy study performed on the *a*-Zr_9Ni_{91} alloy[23] indicated a band structure corresponding to what can be expected on the basis of the calculated DOS for *a*-$Zr_{15}Ni_{85}$.[6] Both the crystalline $ZrNi_5$ compound and the *a*-$Zr_{15}Ni_{85}$ alloy was predicted by DOS calculations[6] to be nonferromagnetic. The magnetic susceptibility measurements on the crystalline $ZrNi_5$ compound[5] have also indicated the absence of ferromagnetism (at least down to 4.2 K).

On the other hand, it can be established on the basis of the DOS curves calculated[6] for the crystalline $ZrNi_5$ compound (83.3 at. % Ni) and the *a*-$Zr_{15}Ni_{85}$ alloy that the basic features of the DOS remain very much the same for both structural modifications (apart from a smearing out of the DOS in the amorphous state with respect to the crystalline phase). The main reason for this is that in the Ni-rich $ZrNi_5$ compound, the elementary cell contains a large number of atoms and, anyway, at such a high Ni content the contribution of Ni atoms dominates the total DOS.

These results suggest that those physical properties which are determined by the DOS curves will mainly depend on the Ni content only in these systems. This could already be seen in Sec. III A and III B. The T_C was higher for larger Ni content in the amorphous Zr-Ni alloys and was nearly equal for the amorphous and bcc Zr-Ni alloys of the same composition. It has been pointed out previously[24] that the shape of the DOS curve is very similar for Zr and Hf metals for a given structural modification, apart from a larger bandwidth

for Hf due to the larger core of $4f$ electrons. This means that the DOS of Ni-rich Hf-Ni alloys will be very similar to those of Zr-Ni alloys with corresponding compositions. Since the DOS around E_F is dominated by the Ni contribution at these high Ni contents, the larger bandwidth of Hf will have little effect only.

Again with reference to the calculated DOS curve of crystalline $ZrNi_5$ and a-$Zr_{15}Ni_{85}$,[6] it can be established that not only the main features of the DOS curves depend on the Ni content but even many of the details of the DOS curve variation around the Fermi level are fairly independent of the atomic arrangements. This is in line with our previous reports[25,26] according to which the electrical transport properties (thermopower, electrical resistivity, and their temperature dependence) are very similar for all the alloys investigated here.

The above considerations about the DOS of Ni-rich (Zr,Hf)-Ni phases will form the basis for our subsequent discussion of the composition dependence of the magnetic properties for these systems in the next section.

B. Composition dependence of magnetic properties of (Zr,Hf)-Ni metastable phases around the PM-FM transition

In the framework of the itinerant electron model of Stoner, the onset of FM corresponds to an exchange splitting of the spin-up and spin-down subbands of d-electron bands. In this model the Curie point is proportional to the exchange splitting and the difference between the number of the spin-up and spin-down d electrons in the two subbands each filled up to energies below the Fermi level equals the magnetic moment. A low Curie point corresponds to small splitting and therefore the magnetic moment will also be small. This case is described by the Stoner-Edwards-Wohlfarth (SEW) model[11] of VWIF of spatially homogeneous ferromagnets. Generally, Ni-based alloys around the critical concentration of the PM-FM transition well obey this theory. We have successfully discussed the behavior of amorphous Ni-P alloys[17] in this framework. All this justifies the analysis of experimental results on Zr-Ni alloys in Sec. III on the basis of Arrott plots derived from the SEW model. This is valid at least for our two amorphous Zr-Ni alloys for which very close T_C values were derived from the ac susceptibility and low-field magnetization measurements as well as from the Arrot plot whereas an overestimated Curie point resulted from the Arrott plot for the spatially much less homogeneous bcc-Ni(Zr) alloy.

It has been shown[27,28] that if the SEW model applies, then the quantities $\sigma^2(0,0)$ and T_C^2 as deducted from the Arrott plots should be a linear function of the concentration of the magnetic constituents. These so-called Mathon plots[27,28] are shown for the Zr-Ni alloys in Fig. 9(a) (T_C^2 vs x_{Ni}) and Fig. 9(b) [$\sigma^2(0,0)$ vs x_{Ni}] where also data from previous studies are included.

For sputtered FM amorphous Zr-Ni alloys, Morel *et al.*[10] derived higher Curie temperatures than our data. A reason for the difference with respect to our results may be due to the fact that in the case of sputtering, there may be a stronger

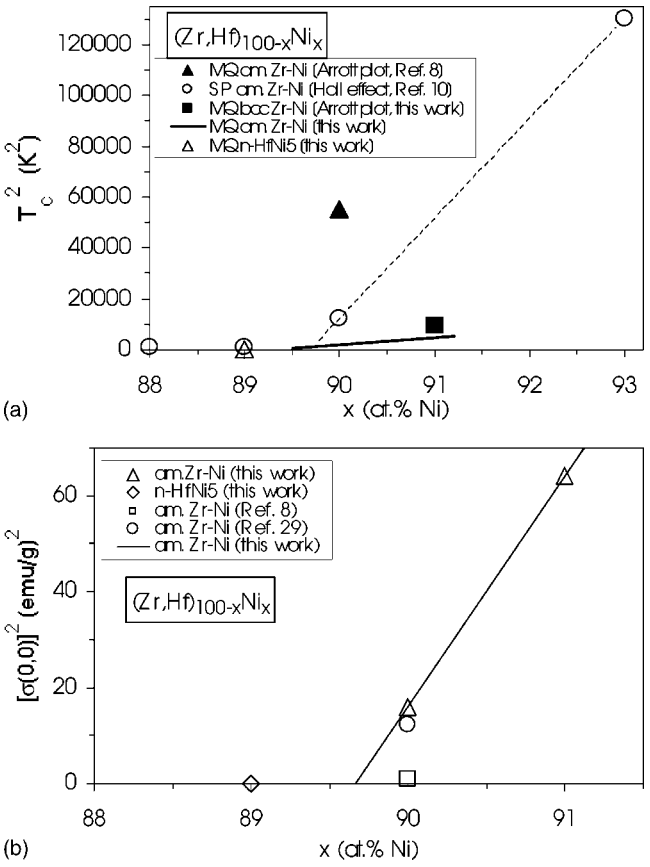

FIG. 9. Mathon plots for the investigated (Zr,Hf)-Ni alloy system: (a) T_C^2 vs x_{Ni} and (b) $\sigma^2(0,0)$ vs x_{Ni}. Relevant data for the Curie temperature from Refs. 8 and 10 and for the saturation magnetization from Refs. 8 and 29 are also included as indicated in the appropriate legends. The solid line indicates a fit to all our T_C data (see Secs. III A and III B) except the T_C value of the bcc ribbon Zr_9Ni_{91} derived from the Arrott plot (symbol ■).

disorder, including also a chemical one, present in the alloy in comparison with the melt-quenched alloy where the chemical interaction can effectively govern the chemical short-range order. Therefore, in the sputtered alloy, regions with Ni contents much higher than the average matrix concentration and thus with higher Curie point can occur.

As far as the even higher T_C value (235 K) reported by Kaul[8] for a melt-quenched a-$Zr_{10}Ni_{90}$ alloy is concerned, we can only conclude that, although a detailed structural characterization of that particular sample is not known, this observed Curie point value cannot be a characteristic of a homogenous solution of Zr in Ni, either in amorphous or crystalline form. Apparently, this T_C value is close to those we attributed to some residual phases in our alloys (cf. Sec. III A).

On the other hand, Fig. 9(a) suggests that the amorphous Zr-Ni alloys studied in the present work can be considered as a fairly homogeneous solid solution of Zr in Ni since they have a lower T_C than any of the previously investigated amorphous alloys.[8,10] These latter as well as the bcc-Ni(Zr) alloys are spatially much more heterogeneous.

According to Fig. 9(a), the critical concentration of the PM-FM transition in the (Zr,Hf)-Ni system is about

89.5 at. % Ni. This is defined by the intercept of the thick solid line with the concentration axis, i.e., where $T_C=0$ K. This line was determined by linear fit to our *TC* data for the two amorphous and the bcc Zr-Ni alloy by excluding, however, the T_C value determined for the bcc alloy from the Arrott plot. The dashed line in Fig. 9(a) based on the data of Morel *et al.*[10] would define a very similar critical Ni concentration.

Although much less data are available for the saturation magnetization at 0 K [Fig. 9(b)] and also their uncertainty is fairly large, they still define a critical Ni concentration close to 89.5 at. % Ni. Here, the data point for the alloy studied by Kaul[8] is again out of trend.

V. SUMMARY

In the present paper, the magnetic properties of melt-quenched metastable Zr-Ni and Hf-Ni alloys with about 90 at. % Ni content were investigated in a wide range of magnetic fields and temperatures. It was deduced from the variation of the saturation magnetization and the Curie temperature with Ni content that the PM-FM transition in these systems occurs at about 89.5 at. % Ni. The experimental finding that the magnetic state of these metastable systems is practically independent of whether the alloying element is Zr or Hf and it is also insensitive to the actual atomic arrangement, including the structurally disordered amorphous state, was explained on the basis of the electronic band structure of these early-late transition-metal alloys. The magnetically ordered low-temperature state could be described by the behavior of spatially homogeneous very weak itinerant ferromagnets (VWIF).

Differences in the magnetic characteristics of the metastable alloys investigated here could only be revealed when analyzing in detail the magnetic contribution of regions more rich in Ni than the alloy matrix itself. These magnetic inhomogeneities form during the preparation process and their amount was actually fairly small except for the bcc-Zr_9Ni_{91} alloy prepared at the lowest quench rate. In previous studies on melt-quenched and sputtered Zr-Ni amorphous alloys much higher Curie temperatures have been observed than in our alloys with the same Ni content and this finding could be ascribed to larger amount of Ni-rich inhomogeneities in those previously investigated samples.

ACKNOWLEDGMENTS

Work supported by the Hungarian Scientific Research Fund (OTKA) through Grant Nos. T 022124 and T 038383. One of the authors (E.V.) acknowledges financial support from the Hungarian Academy of Sciences.

*Corresponding author. E-mail address: bakonyi@szfki.hu
†Present address: Department of Astronomy, Eötvös University, Budapest.

[1] A. Amamou, F. Gautier, and B. Loegel, J. Phys. F: Met. Phys. **5**, 1342 (1975).
[2] F. Acker and R. Huguenin, J. Magn. Magn. Mater. **12**, 58 (1979).
[3] A. Liénard and J. P. Rebouillat, J. Appl. Phys. **49**, 1680 (1978).
[4] A. Fujita, T. H. Chiang, N. Kataoka, and K. Fukamichi, J. Phys. Soc. Jpn. **62**, 2579 (1993).
[5] A. Amamou, R. Kuentzler, Y. Dossmann, P. Forey, J. L. Glimois, and J. L. Feron, J. Phys. F: Met. Phys. **12**, 2509 (1982).
[6] I. Turek, Ch. Becker, and J. Hafner, J. Phys.: Condens. Matter **4**, 7257 (1992).
[7] Z. F. Dong, K. Lu, R. Lück, I. Bakonyi, and Z. Q. Hu, Nanostruct. Mater. **9**, 363 (1997).
[8] S. N. Kaul, Phys. Rev. B **27**, 6923 (1983).
[9] I. Bakonyi, V. Skumryev, R. Reisser, G. Hilscher, L. K. Varga, L. F. Kiss, H. Kronmüller, and R. Kirchheim, Z. Metallkd. **88**, 117 (1997).
[10] R. Morel, L. Abadli, and R. W. Cochrane, J. Appl. Phys. **67**, 5790 (1990).
[11] D. M. Edwards and E. P. Wohlfarth, Proc. R. Soc. London, Ser. A **303**, 127 (1968).
[12] I. Bakonyi, F. Mehner, M. Rapp, Á. Cziráki, H. Kronmüller, and R. Kirchheim, Z. Metallkd. **86**, 619 (1995).
[13] Á. Cziráki, B. Fogarassy, G. Van Tendeloo, P. Lamparter, M. Tegze, and I. Bakonyi, J. Alloys Compd. **210**, 135 (1994).
[14] K. Lu, Z. F. Dong, I. Bakonyi, and Á. Cziráki, Acta Metall. Mater. **43**, 2641 (1995).
[15] R. Lück, Z. F. Dong, M. Schieffer, I. Bakonyi, and K. Lu, Philos. Mag. B **79**, 163 (1999).
[16] J. Gubicza, G. Ribárik, I. Bakonyi, and T. Ungár, J. Nanosci. Nanotechnol. **1**, 343 (2001).
[17] I. Bakonyi, A. Burgstaller, W. Socher, J. Voitländer, E. Tóth-Kádár, A. Lovas, H. Ebert, E. Wachtel, N. Willmann, and H. H. Liebermann, Phys. Rev. B **47**, 14 961 (1993).
[18] L. F. Kiss, I. Bakonyi, A. Lovas, M. Baran, and J. Kadlecová, Phys. Rev. B **64**, 064417 (2001).
[19] G. Herzer, Scr. Metall. Mater. **33**, 1741 (1995).
[20] F. Herman and S. Skillman, *Atomic Structure Calculations* (Prentice-Hall, Inc., Englewood Cliffs, NJ, 1963).
[21] I. Bakonyi, J. Non-Cryst. Solids **180**, 131 (1995).
[22] V. L. Moruzzi, P. Oelhafen, A. R. Williams, R. Lapka, H.-J. Guntherodt, and J. Kübler, Phys. Rev. B **27**, 2049 (1983).
[23] P. Oelhafen, Mater. Sci. Eng. **99**, 239 (1988).
[24] I. Bakonyi, H. Ebert, and A. I. Liechtenstein, Phys. Rev. B **48**, 7841 (1993).
[25] J. Tóth, I. Bakonyi, G. Hilscher, Europhys. Lett. **24**, 379 (1993).
[26] I. Bakonyi, E. Tóth-Kádár, and R. Kirchheim, Z. Metallkd. **86**, 784 (1995).
[27] J. Mathon, Proc. R. Soc. London, Ser. A **306**, 355 (1968).
[28] H. L. Alberts, J. Beille, D. Bloch, and E. P. Wohlfarth, Phys. Rev. B **9**, 2233 (1974).
[29] S. Ohnuma, K. Shirakawa, M. Nose, and T. Masumoto, IEEE Trans. Magn. **16**, 910 (1980).